Transverse and longitudinal lattice modulations in the charge-orbital-ordered manganite $Sr_{2-x}La_xMnO_4$ around $x = 0.5$

Masazumi Arao,[1] Yasuhide Inoue,[1,2] Kensei Toyoda,[3] and Yasumasa Koyama[3]

[1]*Materials Analysis Center, Research Department, NISSAN ARC, LTD., Yokosuka, Kanagawa 237-0061, Japan*

[2]*Center for Crystal Science and Technology, University of Yamanashi, Kofu, Yamanashi 400-8511, Japan*

[3]*Department of Electronic and Photonic Systems and Kagami Memorial Laboratory for Materials Science and Technology, Waseda University, Shinjuku, Tokyo 169-8555, Japan*

(Received 6 December 2009; revised manuscript received 13 June 2011; published 15 July 2011)

For $Sr_{2-x}La_xMnO_4$, having a nearly two-dimensional electronic system of e_g electrons, we have examined the crystallographic features of the charge-orbital-ordered (COO) and charge-exchange (CE)-type magnetic states for $0.40 \leqslant x \leqslant 0.55$ by transmission electron microscopy. Incommensurate and commensurate longitudinal lattice modulations were found below ~150 K for $0.47 \leqslant x \leqslant 0.51$, while the cooling from the disordered tetragonal state resulted in the appearance of transverse modulations below T_{COO} for $0.40 \leqslant x \leqslant 0.52$. For $0.47 \leqslant x \leqslant 0.51$, thus, the longitudinal and transverse modulations were present in both the lower-temperature region of the COO state and the CE-type magnetic state. In addition to these two states, the COO state for $0.40 \leqslant x < 0.47$ and $0.51 < x \leqslant 0.52$ accompanies only the transverse modulation and should be referred to as the orbital modulated state without a charge modulation.

DOI: 10.1103/PhysRevB.84.014102 PACS number(s): 75.47.Lx, 61.50.Ks, 68.37.Lp, 71.45.Lr

The strontium manganite Sr_2MnO_4 consisting of only Mn^{4+} ions has the layered K_2NiF_4-type crystal structure characterized by an isolated MnO_2 layer. Because of the isolated layer, its electronic state can be regarded as a nearly two-dimensional system with an electronic configuration of $t_{2g}{}^3$ for each Mn^{4+} site.[1,2] The $t_{2g}{}^3$ configuration leads to a local magnetic moment at an Mn site. Sr_2MnO_4 was previously reported to exhibit a nearly two-dimensional antiferromagnetic ordering below ~150 K.[2] When Sr^{2+} ions in Sr_2MnO_4 are partially replaced by trivalent rare-earth ions, e_g electrons are introduced into such a system. Our interest is thus focused on both site and orbital occupations of e_g electrons in the nearly two-dimensional electronic system.

To understand the features of site and orbital occupations of e_g electrons, we have so far investigated the crystallographic features of $Sr_{2-x}R_xMnO_4$ with $R^{3+} = Nd^{3+}$, Pr^{3+}, and La^{3+} by transmission electron microscopy.[3–8] It was found that, when the R content x corresponding to the e_g-electron concentration was increased from $x = 0$, in the Nd and Pr cases, the orbital-ordered (OO) state appeared around $x = 0.15$ and was then converted into the charge-orbital-ordered (COO) state around $x = 0.25$, which was present until $x = 0.44$. The COO state is characterized by a lattice modulation with only a transverse-wave character. Because of this feature, it would appear that the COO state can be regarded as an orbital-modulated (OM) state without charge ordering.

In contrast, for the La case, it was reported that the COO state was observed in the range of $0.25 \leqslant x \leqslant 0.50$ and that the charge-exchange (CE)-type magnetic state appeared below T_N of ~110 K at $x = 0.5$.[9–25] The lattice modulation in the CE-type state has both transverse- and longitudinal-wave characters. Our previous study confirmed that the COO state for $0.25 \leqslant x \leqslant 0.44$ is characterized by only the transverse modulation, just as in the Nd and Pr cases, but the nature of the modulation in the COO state around $x = 0.50$ seems to be different from that for $0.25 \leqslant x \leqslant 0.44$. To clarify the validity of this hypothesis, we have investigated the features of the lattice modulation in the COO state of $Sr_{2-x}La_xMnO_4$ around $x = 0.5$ by *in situ* observation using a transmission electron microscope. The detailed experimental data regarding the modulation in the La case, which were obtained in this study, are described here.

In addition to $Sr_{2-x}La_xMnO_4$, the CE-type magnetic state has also been reported in $Ca_{2-x}R_xMnO_4$.[26–29] The difference between the states in $Sr_{2-x}La_xMnO_4$ and $Ca_{2-x}R_xMnO_4$ is that the crystal structures of the latter manganites involve the rotational displacements of oxygen octahedra, which are the same as those found in the La-cuprate superconductors, such as $La_{2-x}Ba_xCuO_4$. The rotational displacements involved in the *Pccn* and low-temperature tetragonal states of the La cuprates are known to result in the suppression of superconductivity.[30–32] In the layered K_2NiF_4-type manganites, thus, the rotational displacement may influence the stability for the OO-, COO-, and CE-type states. To avoid the involvement of an additional factor, in this study, we focus on the electronic states only in $Sr_{2-x}La_xMnO_4$, where no rotational displacement is involved.

$Sr_{2-x}La_xMnO_4$ samples with $0.40 \leqslant x \leqslant 0.55$ were prepared by the coprecipitation technique using citric acid. The sample preparation procedure was described in detail in our previous paper.[3] The crystallographic features of the prepared samples were examined mainly by transmission electron microscopy. Specifically, *in situ* observation was carried out in the temperature range between 15 K and room temperature, using a JEM-3010 transmission electron microscope with a cooling holder equipped with a liquid He reservoir. Thin specimens for observation were prepared by the Ar-ion thinning technique.

When the temperature was lowered from the high-temperature disordered tetragonal (DT) state at $x = 0.50$, the CE-type magnetic state appeared below T_N in the COO state that was characterized by a lattice modulation with $\mathbf{q} = (1/4)[110]_{DT}$. Figure 1 shows two electron-diffraction patterns of the CE-type magnetic state in an $x = 0.50$ sample at 15 K. The pattern with the $[001]_{DT}$ electron incidence in

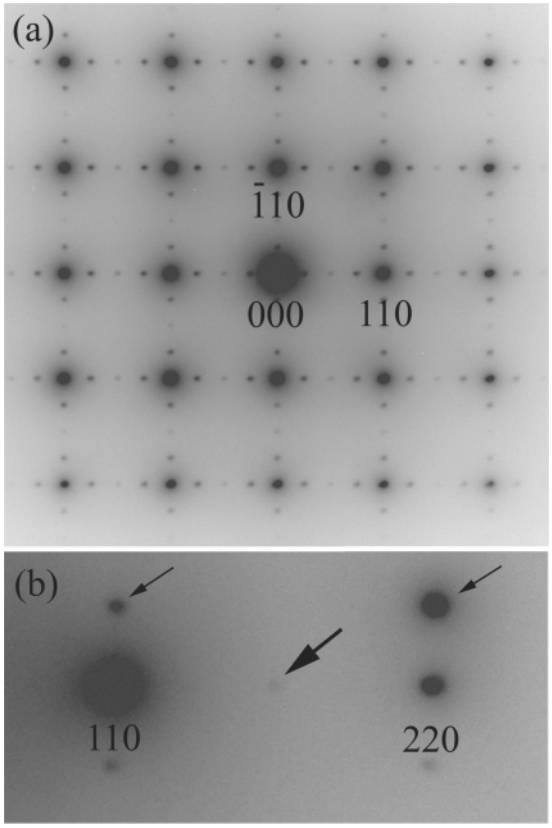

FIG. 1. (a) Electron-diffraction pattern of the CE-type magnetic state in a $Sr_{1.5}La_{0.5}MnO_4$ sample at 15 K. The pattern in (b) was obtained by slightly rotating the sample from the $[001]_{DT}$ electron incidence for (a) in the $[110]_{DT}$ direction. The subscript DT denotes the disordered tetragonal structure. In (b), superlattice reflections with $\mathbf{q} = (1/2)[110]_{DT}$ are present in the $[110]_{DT}$ lines through the origin, in addition to transverse reflections with $\mathbf{q} = (1/4)[110]_{DT}$. This is indicative of the fact that a longitudinal lattice modulation is present in the CE-type magnetic state.

Fig. 1(a) exhibits weak superlattice reflections at both $\mathbf{q} = (1/4)[110]_{DT}$ and $\mathbf{q} = (1/2)[110]_{DT}$, in addition to strong fundamental reflections due to the DT state. The features found in the pattern are entirely consistent with those obtained in the previous studies.[2,9,10,13]

Among these features, the reflection at $\mathbf{q} = (1/2)[110]_{DT}$ seems to be the second-order harmonics of that at $\mathbf{q} = (1/4)[110]_{DT}$. To confirm this, we slightly rotated the sample in the $[110]_{DT}$ direction to avoid double diffraction and then took the pattern in Fig. 1(b). The notable feature found in Fig. 1(b) is that only the 1/2-type reflections are detected in the $[110]_{DT}$ symmetry line through the origin 000, as indicated by the thick arrows. The 1/4-type reflections marked by the thin arrows are, on the other hand, present in the $[\bar{1}10]_{DT}$ line through each $hh0_{DT}$ reflection. Based on the extinction rule of $\mathbf{g} \cdot \mathbf{e} = 0$ for a lattice modulation, where $\mathbf{g}$ and $\mathbf{e}$ denote a scattering vector and a displacement vector of a modulation, it is clear that the 1/4-type and 1/2-type superlattice reflections basically originate from transverse and longitudinal lattice modulations, respectively. This means that both the longitudinal modulation and the second-order harmonics of the transverse modulation contribute to the 1/2-type reflection. Because the longitudinal modulation with a periodicity of $2d_{110}$ can be strongly coupled to a charge, the CE-type magnetic state should be characterized by a charge modulation, together with an orbital modulation related to the transverse modulation with a periodicity of $4d_{110}$, where d_{110} is a spacing of the $(110)_{DT}$ plane.

Here, it should be remarked that the presence of the 1/4- and 1/2-type superlattice reflections in the $[110]_{DT}$ symmetry line have been reported in the synchrotron-radiation[9,10,18,19] and electron-diffraction[1,2,13] experiments, while the neutron-diffraction experiments exhibited only the 1/2-type reflections.[14–17] In our electron-diffraction patterns, in fact, the 1/4- and 1/2-type reflections were observed for the $[001]_{DT}$ electron incidence, as shown in Fig. 1(a). However, the 1/4-type reflection is absent in Fig. 1(b). This implies that the double-diffraction effect results in the appearance of the 1/4-type reflections in the $[110]_{DT}$ symmetry line through the origin. It is thus understood that our experimental data are quite consistent with the neutron-diffraction result, rather than the synchrotron one.

In $Sr_{2-x}R_xMnO_4$ with R = Nd, Pr, and La, the COO state in $0.25 \leqslant x \leqslant 0.44$ is characterized by only a transverse modulation with a wave vector of $\mathbf{q} = [\zeta\ \zeta\ 0]_{DT}$, and should be referred to as the OM state without a charge modulation. In view of this result, our interest is next focused on the e_g-electron-concentration range in the La case, in which the longitudinal modulation is present. We examined the features of lattice modulations in $Sr_{2-x}La_xMnO_4$ with $0.40 \leqslant x \leqslant 0.55$ at 15 K. Figure 2 shows electron-diffraction patterns for $x = 0.44$, 0.47, 0.49, 0.50, and 0.51 together with their corresponding intensity profiles along the $[110]_{DT}$ line through the origin. To avoid double diffraction, the samples were slightly rotated in the $[110]_{DT}$ direction from the $[001]_{DT}$ electron incidence. It should be remarked that, because the patterns, except for $x = 0.47$, were obtained from areas including two variants, superlattice reflections due to the transverse modulation are still present in the $[\bar{1}10]_{DT}$ line through each fundamental reflection, as indicated by the arrows in Fig. 2 (a). On the other hand, the patterns for $x = 0.47$ involve only the contribution of a single variant with $\mathbf{q} = [\zeta\ \zeta\ 0]_{DT}$. In this figure then we show two electron-diffraction patterns for $x = 0.47$. The electron beam incidence of one pattern in Fig. 2(b) is parallel to the $[001]_{DT}$ direction, while the other in Fig. 2(c) was obtained by rotating the sample to avoid double diffraction.

Both the pattern and the profile for $x = 0.44$ indicate that there is no superlattice reflection in the $[110]_{DT}$ line through the origin 000, although extremely weak diffuse scattering can be detected at a position of $\zeta = 0.44$. The presence of the superlattice reflections at positions marked by the arrows in Fig. 2(a) confirms that the COO state is characterized by only the transverse lattice modulation with a wave vector of $\mathbf{q} = [\zeta\ \zeta\ 0]_{DT}$ with $\zeta = 0.22$, just as in the Nd and Pr cases. For $0.47 \leqslant x \leqslant 0.51$, on the other hand, superlattice reflections due to the longitudinal modulation are present in the patterns and the profiles. The notable feature is that, unlike the 1/2-type reflections for $x = 0.50$ and 0.51, the reflections for $x = 0.47$ and 0.49 are, respectively, located at incommensurate positions of $\zeta = 0.47$ and 0.49, as indicated by the arrows. The presence of the incommensurate periodicity is indicative of the fact that the longitudinal modulation should be due to the charge

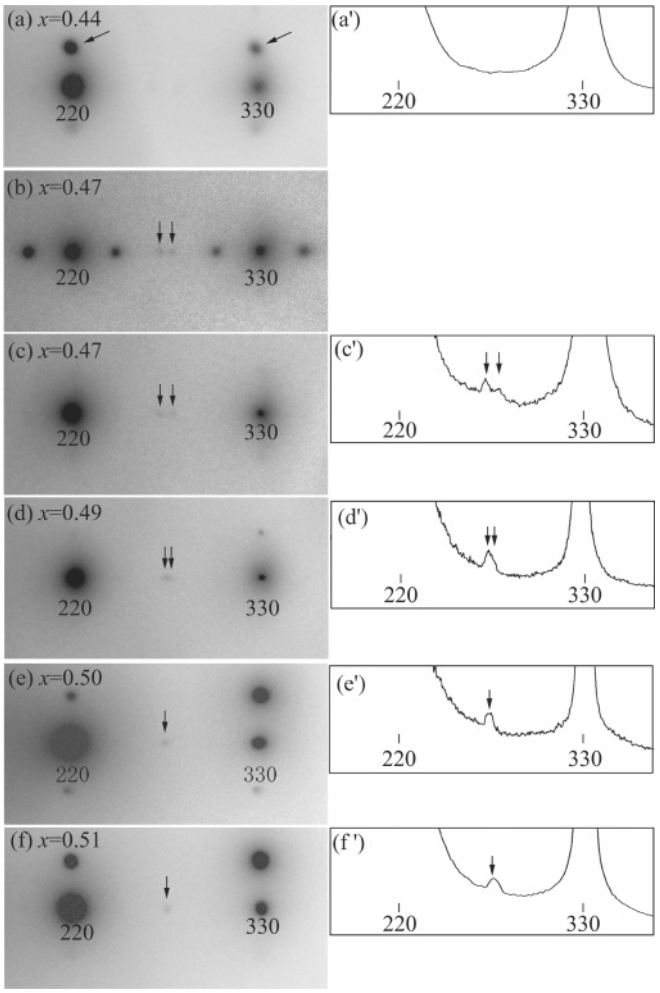

FIG. 2. Electron-diffraction patterns of samples with (a) $x = 0.44$, (b) and (c) $x = 0.47$, (d) $x = 0.49$, (e) $x = 0.50$, and (f) $x = 0.51$ at 15 K together with their corresponding intensity profiles in (a′), (c′), (d′), (e′), and (f′). To avoid double diffraction, the patterns, except for $x = 0.47$, obtained from areas consisting of two variants, were taken by slightly rotating the samples from the $[001]_{DT}$ electron incidence. On the other hand, a single-variant region contributed to diffraction patterns for $x = 0.47$ and then two patterns for $x = 0.47$ are shown in the figure. One in (b) has the electron beam incidence parallel to the $[001]_{DT}$ direction, while the other in (c) was obtained by rotating the sample to avoid double diffraction. In addition, the intensity profiles of these patterns were also measured along the $[110]_{DT}$ direction through the origin 000. As indicated by the arrows in each profile, the superlattice reflections due to the longitudinal modulation are clearly seen in $0.47 \leqslant x \leqslant 0.51$.

modulation rather than charge ordering for an integer charge. It was eventually found that the longitudinal modulation at 15 K was present only for $0.47 \leqslant x \leqslant 0.51$, while the COO state for both $0.40 \leqslant x < 0.47$ and $0.51 < x \leqslant 0.52$ was confirmed to be identified as the OM state without a charge modulation.

The periodicities of the transverse and longitudinal lattice modulations at 15 K were determined from the locations of the superlattice reflections present in Fig. 2. The ζ values of the modulations with $\mathbf{q} = [\zeta\ \zeta\ 0]_{DT}$ are actually plotted as a function of the La content x in Fig. 3. From Fig. 3, when the La content increases between $x = 0.44$ and 0.52, the ζ values

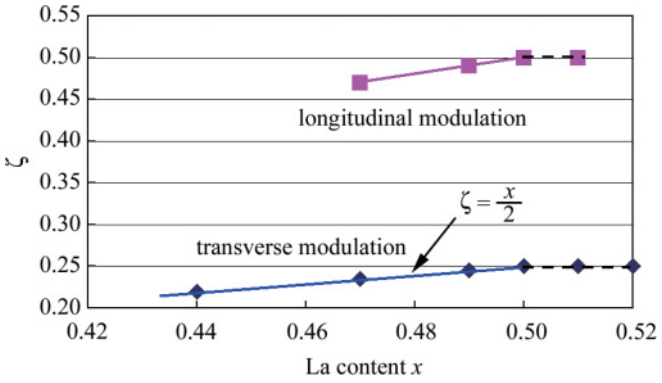

FIG. 3. (Color online) Variation in the ζ values of the longitudinal and transverse lattice modulations at 15 K in the La content between $x = 0.44$ and 0.52. A wave vector of a modulation is specified as $\mathbf{q} = [\zeta\ \zeta\ 0]_{DT}$, and each ζ value plotted here was determined from the location of the superlattice reflection in Fig. 2. In the figure, the red and blue squares represent the determined ζ values of the longitudinal and transverse modulations, respectively. The relation between the transverse ζ value and the La content x is confirmed to be expressed by $\zeta = x/2$. It is understood that the longitudinal modulation is present at 15 K in $0.47 \leqslant x \leqslant 0.51$ and that the ζ value of the longitudinal modulation is twice as that of the transverse one.

of the longitudinal and transverse lattice modulations increase linearly for $x < 0.50$ and then reach the constant values of $\zeta = 0.50$ and 0.25 for $x = 0.50$, respectively. The values of $\zeta = 0.50$ and 0.25 for $x = 0.51$ are the same as those for $x = 0.50$. Note that the ζ value of the longitudinal modulation is twice that of the transverse one. The following should be remarked here: in Fig. 3, the relation between the transverse ζ value and the La content x is confirmed to be expressed by $\zeta = x/2$. That is, the confirmation of this relation is an experimental indication that the prepared samples have good qualities, even for surface stoichiometry.

$Sr_{1.5}La_{0.5}MnO_4$ exhibits the (DT $\rightarrow$ COO) transition at T_{COO} of $\sim$240 K, and the CE-type magnetic state appears at T_N of $\sim$110 K in the COO state.[11,12] To understand the difference between successive transitions in $x = 0.50$ and 0.51, we examined the crystallographic features of the $x = 0.51$ sample in the temperature range between 15 K and room temperature. Figure 4 shows three electron-diffraction patterns taken from (a) the high-temperature DT state at 170 K, (b) the COO state at 150 K, and (c) the CE-type state at 89 K for $x = 0.51$. To avoid double diffraction, the sample was slightly rotated in the $[110]_{DT}$ direction from the $[001]_{DT}$ electron incidence. The insets in each figure show the corresponding intensity profiles along the $[110]_{DT}$ symmetry line. Even at 170 K in Fig. 4 (a), there are only fundamental reflections due to the DT state, although strong diffuse scattering is present at the 1/4-type position. When the temperature is lowered from the DT state, 1/4-type superlattice reflections appear at T_{COO} of $\sim$160 K, as indicated by the arrows in Fig. 4(b). The important feature of the pattern at 150 K is that there is no longitudinal reflection in the $[110]_{DT}$ line through the origin. The further cooling from 150 K results in the appearance of 1/2-type reflections, as indicated by the arrows in Fig. 4(c) and its inset. That is, both the transverse and longitudinal modulations are present in the CE-type magnetic state. The point to note

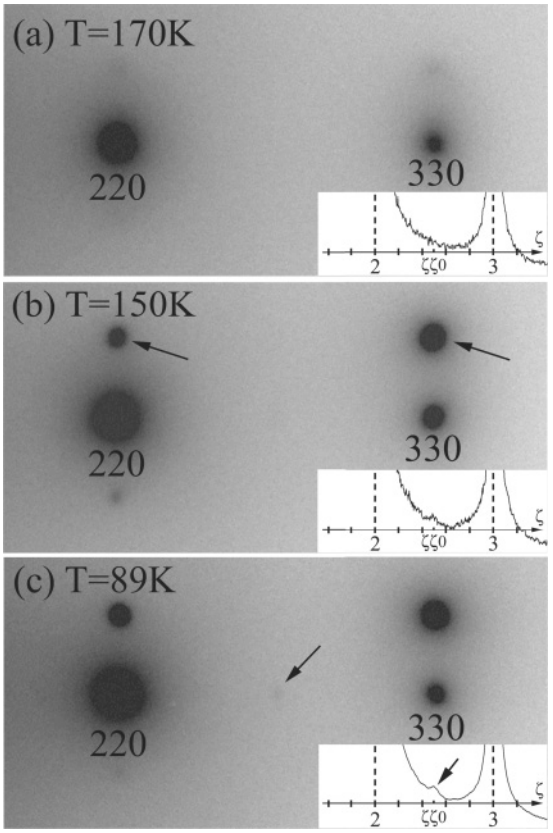

FIG. 4. Electron-diffraction patterns of (a) the DT state at 170 K, (b) the COO state at 150 K, and (c) the CE-type magnetic state at 89 K for $x = 0.51$ together with their corresponding intensity profiles along the $[110]_{DT}$ direction in their inset. The electron beam incidence for these patterns is nearly parallel to the $[001]_{DT}$ direction. As seen in the patterns, the CE-type magnetic state is characterized by both the transverse 1/4-type and longitudinal 1/2-type superlattice reflections.

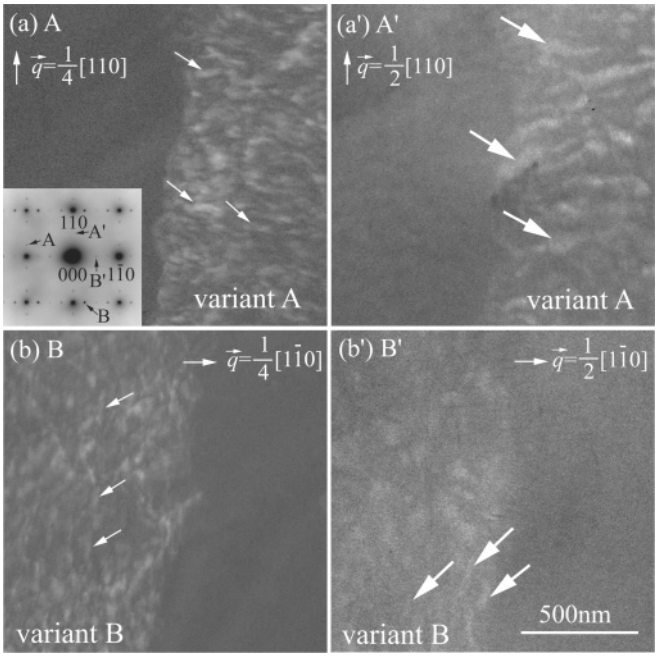

FIG. 5. Dark field images showing transverse- and longitudinal-modulation regions in the CE-type state at 89 K for $x = 0.51$. The images in (a), (a′), (b), and (b′) were, respectively, taken by the superlattice reflections marked by arrows A, A', B, and B' in the corresponding $[001]_{DT}$ diffraction pattern in the inset. Note that, in taking each image, the sample was slightly rotated from the $[001]_{DT}$ incidence to avoid double diffraction. In (a) and (b) for the transverse modulation, there are two transverse variants, which are referred to as A and B variants. Longitudinal regions in the A and B variants are observed in (a′) and (b′), respectively. The disagreement between the spatial distributions of the transverse and longitudinal regions in each variant suggests that the appearance of the longitudinal modulation is not strongly influenced by the presence of the transverse modulation.

here is that T_{COO} for $x = 0.51$ is ∼80 K lower than that for $x = 0.50$.

Four dark field images indicating the spatial distributions of both the transverse- and longitudinal-modulation regions in the same area of the CE-type magnetic state at 89 K for $x = 0.51$ are shown in Fig. 5 together with a corresponding $[001]_{DT}$ electron-diffraction pattern in the inset. The images in Fig. 5(a), 5(a′), 5(b), and 5(b′) were taken by using the reflections indicated by arrows A, A', B, and B' in the pattern, respectively. When the wave vector for A is assumed to be $\mathbf{q} = (1/4)[110]_{DT}$, the vectors for A', B, and B' are specified as $\mathbf{q} = (1/2)[110]_{DT}$, $\boldsymbol{q} = (1/4)[1\bar{1}0]_{DT}$, and $\boldsymbol{q} = (1/2)[1\bar{1}0]_{DT}$, respectively.

We first look at the images in Figs. 5(a) and 5(b) for the transverse modulation. Transverse regions for two variants, which are here called the A and B variants, are seen as bright contrast in Figs. 5(a) and 5(b), respectively. These two transverse variants are separated by a curved boundary, and small-sized regions giving rise to strong bright contrast are also detected in each variant, as indicated by the thin arrows. The presence of the small-sized regions presumably indicates that a spatial fluctuation of the transverse modulation should be involved in each variant. Longitudinal regions in the A and B variants are, on the other hand, observed as bright-contrast regions in Figs. 5(a′) and 5(b′), respectively. Both the shape and distribution of longitudinal regions are not identical to those of the small-sized regions in the transverse variants. The interesting feature is that longitudinal regions in each transverse variant are somewhat elongated along a direction perpendicular to the $\mathbf{q}$ vector, as indicated by the thick arrows. This suggests that the longitudinal modulation reflecting a charge modulation tends to develop easily along such a perpendicular direction.

Because of the strong suppression of T_{COO}, for $x = 0.51$, it was hard to check whether the longitudinal modulation was present or not in $T_N \leqslant T \leqslant T_{COO}$. We then examined the presence of the longitudinal reflection in the COO state by using the $x = 0.49$ sample. Note that T_{COO} and T_N for $x = 0.49$ were, respectively, determined to be ∼250 K and ∼100 K. Figure 6 shows three electron-diffraction patterns at (a) 160 K, (b) 140 K, and (c) 120 K for $x = 0.49$, together with their corresponding intensity profiles along the $[110]_{DT}$ symmetry line in their insets. To avoid double diffraction, the sample was slightly rotated in the $[110]_{DT}$ direction from the $[001]_{DT}$ electron incidence. There is no longitudinal reflection in the pattern in Fig. 6(a) at 160 K. At 140 K and 120 K, on the other hand, we can detect longitudinal reflections with the incommensurate periodicity, as indicated by the arrows in

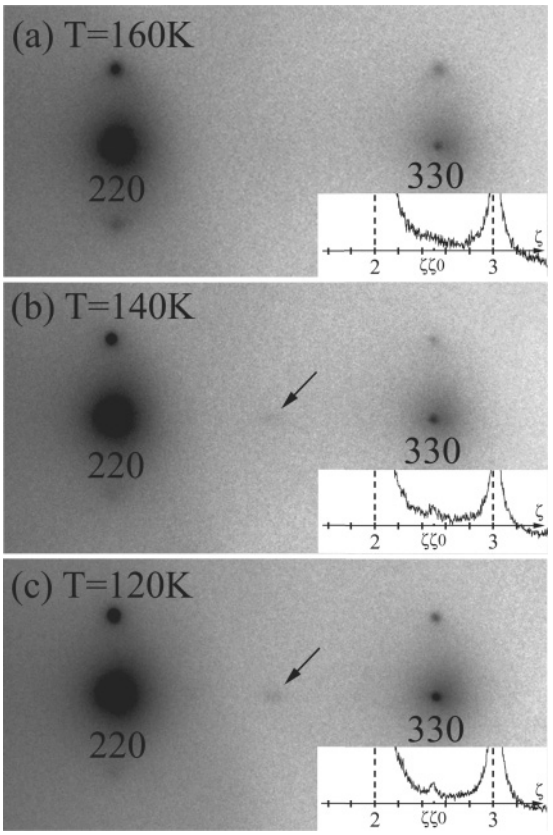

FIG. 6. Electron-diffraction patterns taken at (a) 160 K, (b) 140 K, and (c) 120 K in the COO state for $x = 0.49$ together with their corresponding intensity profiles along the $[110]_{DT}$ direction in their inset. Their electron beam incidence is nearly parallel to the $[001]_{DT}$ direction. Incommensurate longitudinal reflections are present below ~150 K in the COO state, as indicated by the arrows in (b) and (c).

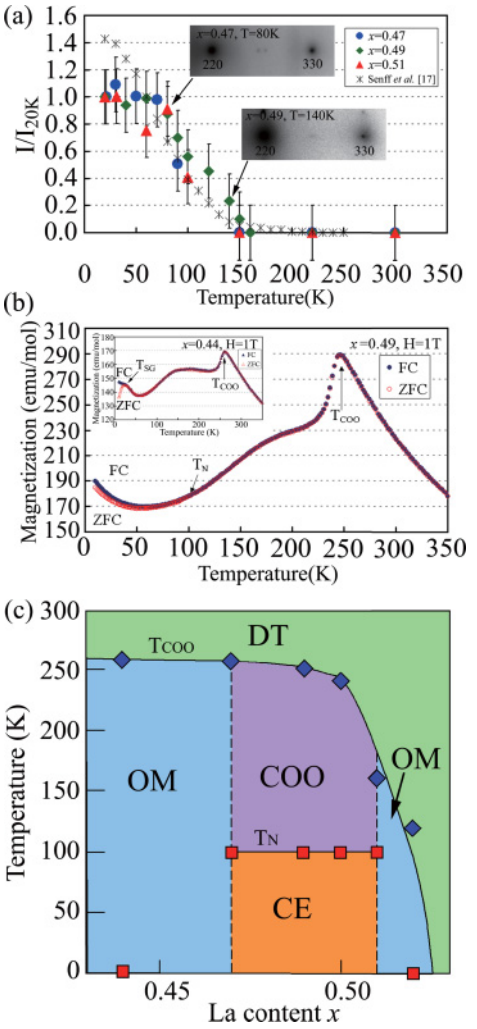

FIG. 7. (Color online) (a) Measured intensities of the $\zeta\ \zeta\ 0$ superlattice reflection as a function of temperature for $x = 0.47$, 0.49, and 0.51 together with diffraction patterns of both the CE-type magnetic state at 80 K for $x = 0.47$ and the COO state at 140 K for $x = 0.49$ in the insets. The measured intensity at each temperature is normalized with respect to that at 20 K. In addition, the CE-correlation intensity for the elastic neutron scattering at each temperature, which was obtained by Senff *et al.*, is also plotted in the figure (see Ref. 17). Note that their intensity at 60 K is assumed to be a unity in the plot. The increase in the intensity from a zero value occurs around 150 K in the COO state. (b) Temperature dependence of the magnetization for $x = 0.49$ together with that for $x = 0.44$ in the inset for the comparison. The peak in the magnetization for $x = 0.44$ and 0.49 corresponds to T_{COO}. The feature of the temperature dependences is that the field cooling (FC) and zero-field cooling (ZFC) curves are separated below ~30 K for $x = 0.44$ and below ~100 K for $x = 0.49$. The latter temperature for $x = 0.49$ can be identified as T_N, while a spin-glass state should appear below the former temperature T_{SG} in $x = 0.44$. (c) Phase diagram determined for $Sr_{2-x}La_xMnO_4$ in the range of $0.43 < x < 0.53$. In the diagram, the disordered tetragonal state, the orbital modulated state, COO state, and the CE-type magnetic state are denoted by DT, OM, COO, and CE, respectively. Among these four states, the OM state accompanies only the transverse modulation, and there exist the transverse and longitudinal modulations in the lower-temperature region of the COO state. The CE-type magnetic state is thus characterized by the introduction of the three-dimensional magnetic ordering in the COO state with the orbital and charge modulations.

Figs. 6(b) and 6(c). It is likely that the longitudinal modulation appears below ~150 K in the COO state.

To construct the phase diagram around $x = 0.5$, we measured intensities of longitudinal reflections at various temperatures in $0.47 \leqslant x \leqslant 0.51$. In Fig. 7(a), measured intensities of the $\zeta\ \zeta\ 0$ superlattice reflection for $x = 0.47$, 0.49, and 0.51 are plotted as a function of temperature. The intensity at each temperature is normalized with respect to that at 20 K. When the temperature is lowered from room temperature, as shown in Fig. 7, an increase in the intensity from a zero value occurs around 150 K. In other words, in the present study, no longitudinal reflection could be detected above ~160 K. In addition, the subsequent cooling below ~60 K does not lead to a remarkable change in the intensity. The notable point is that there is no essential difference among $x = 0.47$, 0.49, and 0.51 with respect to the temperature dependence. Our electron-diffraction data are then compared with the neutron-diffraction data reported by Senff *et al.*[17] In Fig. 7(a), concretely, we plot the intensity of the elastic neutron scattering for the CE correlation at each temperature. Note that their intensity at 60 K is assumed to be a unity in the plot. It is understood that our data are in good agreement with their data between ~150 and ~60 K. In particular, the longitudinal modulation appears at the temperature where the

CE correlation starts to develop in the COO state. Based on the fact that there is no essential difference with respect to temperature dependence and the agreement between the electron- and neutron-diffraction data, T_N is estimated to be ∼100 K for $x = 0.47$, 0.49, and 0.51. To confirm the estimated value of T_N, we measured the magnetization at each temperature for the prepared samples by SQUID. As a result, the obtained behaviors for $x = 0.47$, 0.49, and 0.51 were found to be the same as one another. The temperature dependence for $x = 0.49$ is, as an example, shown in Fig. 7(b) together with that for $x = 0.44$ in the inset. From the figure, the behavior for $x = 0.49$ is understood to be entirely consistent with that for $x = 0.50$, which was reported by Senff *et al.* for a single crystal.[17] In this study, the value of T_N is evaluated as a temperature in which the field cooling (FC) and zero-field cooling (ZFC) curves were separated in the temperature dependence of the magnetization. It was then confirmed that the T_N value for $x = 0.47$, 0.49, and 0.51 was determined to be ∼100 K, as indicated by the arrow in Fig. 7(b) for $x = 0.49$. In addition, the upturn in the magnetization is found to occur below ∼60 K, where our electron-diffraction data deviated from those obtained by the neutron-diffraction experiment, as shown in Fig. 7(a).

The phase diagram for $0.43 < x < 0.53$ constructed in this study is shown in Fig. 7(c). For $0.47 \leqslant x \leqslant 0.51$ in the diagram, the transverse and longitudinal lattice modulations are present in both the lower-temperature region of the COO state for $T_N \leqslant T \leqslant T_{COO}$ and the CE-type magnetic state below T_N. As a result of the presence of the longitudinal modulation in the COO state, thus, the CE-type magnetic state is characterized by the introduction of the three-dimensional magnetic ordering into the COO state with the transverse and longitudinal modulations. Note that the CE correlation in the COO state was pointed out to have a two-dimensional character.[17]

Based on these observations, here, we discuss the origins of the transverse and longitudinal modulations found in this study. The transverse modulation is present in $0.25 \leqslant x \leqslant 0.52$ for the whole COO state and should play a role of a Jahn–Teller distortion for orbital ordering of e_g electrons because it results in the lowering of the symmetry at each Mn site. This speculation can be supported by the group theory. The DT state in $Sr_{2-x}La_xMnO_4$ has tetragonal symmetry. As suggested in our previous studies,[4,5] however, the Jahn–Teller distortion in the OO state around $x = 0.15$ could be associated with the E_g irreducible representation of the O_h group, in the Koster notation,[33] on the basis of a local pseudocubic symmetry of the Mn site. The E_g representation at $\mathbf{q} = 0$ is reduced to the Σ_1 and Σ_4 representations in the Σ symmetry line for $\mathbf{q} = [\zeta\ \zeta\ 0]_{DT}$. Of these two representations, the Σ_4 representation can lead to the transverse modulation as a Jahn–Teller distortion. Based on this, the COO state with only the transverse modulation for both $0.25 \leqslant x < 0.47$ and $0.51 < x \leqslant 0.52$ can be referred to as the OM state, just as in the Nd and Pr cases. For $x < 0.50$, on the other hand, the longitudinal modulation is associated with the identity Σ_1 representation. The different representations obviously lead to the different physical origins. The longitudinal modulation related to the identity representation is compatible with a charge modulation because it is strongly coupled to a charge. It can thus be concluded that both the lower-temperature region of the COO state and the CE-type magnetic state for $0.47 \leqslant x \leqslant 0.51$ is characterized by the orbital and charge modulations.

Brey theoretically discussed the stability of the diagonal phase in simple perovskite manganites in terms of the double-exchange model, including the electron-phonon coupling, the antiferromagnetic interaction, and the on-site Coulomb repulsion.[34] Note that the diagonal phase can be regarded as the COO state in this study. Brey indicated that, in the diagonal phase as a ground state, the inclusion of the on-site Coulomb repulsion or the electron-phonon coupling resulted in a charge density modulation with a single Fourier component. Based on our experimental data, on the other hand, only the CE-type state is characterized by the coexistence of the magnetic ordering and the orbital and charge modulations. It is thus suggested that Brey's model may be responsible for the stabilities of the CE-type magnetic state in $Sr_{2-x}La_xMnO_4$ with $0.47 \leqslant x \leqslant 0.51$, rather than the whole COO state.

In summary, our *in situ* observation on $Sr_{2-x}La_xMnO_4$ revealed that the decrease in temperature for $0.47 \leqslant x \leqslant 0.51$ resulted in the successive structural transitions from the DT state to the COO state and then to the CE-type magnetic state. The notable feature is that both the lower-temperature region of the COO state and the CE-type state are characterized by the presence of the transverse and longitudinal modulations. It is thus understood that the COO state for $0.47 \leqslant x \leqslant 0.51$ should be distinct from the OM state for both $0.25 \leqslant x < 0.47$ and $0.51 < x \leqslant 0.52$, which is characterized by only the transverse modulation. In addition, the transverse modulation can be regarded as a Jahn–Teller distortion for orbital ordering of e_g electrons, while the longitudinal modulation should be the response of a lattice system to a charge modulation. Because the CE correlation has a two-dimensional character in the COO state, the CE-type magnetic state appears by the introduction of the three-dimensional magnetic ordering into the COO state with the orbital and charge modulations.

[1] Y. Moritomo, Y. Tomioka, A. Asamitsu, Y. Tokura, and Y. Matsui, Phys. Rev. B **51**, 3297 (1995).
[2] W. Bao, C. H. Chen, S. A. Carter, and S. W. Cheong, Solid State Commun. **98**, 55 (1996).
[3] W. Norimatsu and Y. Koyama, Phys. Rev. B **74**, 085113 (2006).
[4] W. Norimatsu and Y. Koyama, Phys. Rev. B **75**, 104416 (2007).
[5] W. Norimatsu and Y. Koyama, Phys. Rev. B **75**, 235121 (2007).
[6] W. Norimatsu and Y. Koyama, Physica C **463–465**, 115 (2007).
[7] W. Norimatsu, G. Shindo, and Y. Koyama, Physica B **403**, 1585 (2008).
[8] Y. Inoue, M. Arao, G. Shindo, and Y. Koyama, Mater. Science Forum **638–642**, 1760 (2010).
[9] S. Larochelle, A. Mehta, N. Kaneko, P. K. Mang, A. F. Panchula, L. Zhou, J. Arthur, and M. Greven, Phys. Rev. Lett. **87**, 095502 (2001).

[10]S. Larochelle, A. Mehta, L. Lu, P. K. Mang, O. P. Vajk, N. Kaneko, J. W. Lynn, L. Zhou, and M. Greven, Phys. Rev. B **71**, 024435 (2005).
[11]S. B. Wilkins, P. D. Spencer, P. D. Hatton, S. P. Collins, M. D. Roper, D. Prabhakaran, and A. T. Boothroyd, Phys. Rev. Lett. **91**, 167205 (2003).
[12]S. B. Wilkins, N. Stojić, T. A. W. Beale, N. Binggeli, C. W. M. Castleton, P. Bencok, D. Prabhakaran, A. T. Boothroyd, P. D. Hatton, and M. Altarelli, Phys. Rev. B **71**, 245102 (2005).
[13]L. J. Zeng, C. Ma, H. X. Yang, R. J. Xiao, J. Q. Li, and J. Jansen, Phys. Rev. B **77**, 024107 (2008).
[14]B. J. Sternlieb, J. P. Hill, U. C. Wildgruber, G. M. Luke, B. Nachumi, Y. Moritomo, and Y. Tokura, Phys. Rev. Lett. **76**, 2169 (1996).
[15]D. Senff, P. Reutler, M. Braden, O. Friedt, D. Bruns, A. Cousson, F. Bourée, M. Merz, B. Büchner, and A. Revcolevschi, Phys. Rev. B **71**, 024425 (2005).
[16]D. Senff, F. Krüger, S. Scheidl, M. Benomar, Y. Sidis, F. Demmel, and M. Braden, Phys. Rev. Lett. **96**, 257201 (2006).
[17]D. Senff, O. Schumann, M. Benomar, M. Kriener, T. Lorenz, Y. Sidis, K. Habicht, P. Link, and M. Braden, Phys. Rev. B **77**, 184413 (2008).
[18]Y. Murakami, H. Kawada, H. Kawata, M. Tanaka, T. Arima, Y. Moritomo, and Y. Tokura, Phys. Rev. Lett. **80**, 1932 (1998).
[19]Y. Wakabayashi, Y. Murakami, Y. Moritomo, I. Koyama, H. Nakao, T. Kiyama, T. Kimura, Y. Tokura, and N. Wakabayashi, J. Phys. Soc. Jpn. **70**, 1194 (2001).
[20]S. S. Dhesi, A. Mirone, C. De Nadaï, P. Ohresser, P. Bencok, N. B. Brookes, P. Reutler, A. Revcolevschi, A. Tagliaferri, O. Toulemonde, and G. van der Laan, Phys. Rev. Lett. **92**, 056403 (2004).
[21]D. J. Huang, W. B. Wu, G. Y. Guo, H. J. Lin, T. Y. Hou, C. F. Chang, C. T. Chen, A. Fujimori, T. Kimura, H. B. Huang, A. Tanaka, and T. Jo, Phys. Rev. Lett. **92**, 087202 (2004).
[22]J. Herrero-Martin, J. García, G. Subías, J. Blasco, and M. C. Sánchez, Phys. Rev. B **72**, 085106 (2005).
[23]N. Stojić, N. Binggeli, and M. Altarelli, Phys. Rev. B **72**, 104108 (2005).
[24]K. Kuepper, R. Klingeler, P. Reutler, B. Büchner, and M. Neumann, Phys. Rev. B **74**, 115103 (2006).
[25]M. Merz, G. Roth, P. Reutler, B. Büchner, D. Arena, J. Dvorak, Y. U. Idzerda, S. Tokumitsu, and S. Schuppler, Phys. Rev. B **74**, 184414 (2006).
[26]X. Z. Yu, R. Mathieu, T. Arima, Y. Kaneko, J. P. He, M. Uchida, T. Asaka, T. Nagai, K. Kimoto, A. Asamitsu, Y. Matsui, and Y. Tokura, Phys. Rev. B **75**, 174441 (2007).
[27]S. Chi, F. Ye, P. Dai, J. A. Fernandez-Baca, Q. Huang, J. W. Lynn, E. W. Plummer, R. Mathieu, Y. Kaneko, and Y. Tokura, PNAS **104**, 10796 (2007).
[28]F. Ye, S. Chi, J. A. Fernandez-Baca, A. Moreo, E. Dagotto, J. W. Lynn, R. Mathieu, Y. Kaneko, Y. Tokura, and P. Dai, Phys. Rev. Lett. **103**, 167202 (2009).
[29]D. Okuyama, Y. Tokunaga, R. Kumai, Y. Taguchi, T. Arima, and Y. Tokura, Phys. Rev. B **80**, 064402 (2009).
[30]A. R. Moodenbaugh, Y. Xu, M. Suenaga, T. J. Folkerts, and R. N. Shelton, Phys. Rev. B **38**, 4596 (1988).
[31]M. K. Crawford, R. L. Harlow, E. M. McCarron, W. E. Farneth, J. D. Axe, H. Chou, and Q. Huang, Phys. Rev. B **44**, 7749 (1991).
[32]Y. Inoue, Y. Horibe, and Y. Koyama, Phys. Rev. B **56**, 14176 (1997).
[33]G. F. Koster, *Solid State Physics*, edited by F. Seitz and D. Turnbull, Vol. V (Academic Press Inc., New York, 1957), p. 173.
[34]L. Brey, Phys. Rev. Lett. **92**, 127202 (2004).